Journal of Geophysical Research: Atmospheres

RESEARCH ARTICLE
10.1002/2017JD027109

Exploring the Utility of IASI for Monitoring Volcanic SO_2 Emissions

Isabelle A. Taylor[1], James Preston[2], Elisa Carboni[3], Tamsin A. Mather[1], Roy G. Grainger[3], Nicolas Theys[4], Silvana Hidalgo[5], and Brendan McCormick Kilbride[6]

[1]COMET, Department of Earth Sciences, University of Oxford, Oxford, UK, [2]Department of Earth Sciences, University of Oxford, Oxford, UK, [3]COMET, Sub-Department of Atmospheric, Oceanic and Planetary Physics, University of Oxford, Oxford, UK, [4]Royal Belgian Institute for Space Aeronomy (BIRA-IASB), Brussels, Belgium, [5]Instituto Geofísico de la Escuela Politécnica Nacional, Quito, Ecuador, [6]COMET, Department of Earth Sciences, University of Cambridge, Cambridge, UK

Key Points:
- A fast linear retrieval is applied across the globe to detect sources of sulfur dioxide
- A full iterative retrieval is then conducted over Ecuador and Kamchatka to assess changes in volcanic activity
- The results imply that these retrievals have potential for monitoring weaker emissions of SO_2

Supporting Information:
- Supporting Information S1
- Movie S1

Correspondence to:
I. A. Taylor,
isabelle.taylor@earth.ox.ac.uk

Citation:
Taylor, I. A., Preston, J., Carboni, E., Mather, T. A., Grainger, R. G., Theys, N., et al. (2018). Exploring the utility of IASI for monitoring volcanic SO_2 emissions. *Journal of Geophysical Research: Atmospheres*, *123*, 5588–5606. https://doi.org/10.1002/2017JD027109

Received 11 MAY 2017
Accepted 30 MAR 2018
Accepted article online 6 APR 2018
Published online 16 MAY 2018

Abstract Satellite remote sensing is a valuable method for detecting and quantifying sulfur dioxide (SO_2) emissions at volcanoes. The use of ultraviolet satellite instruments for monitoring purposes has been assessed in numerous studies, but there are advantages to using infrared measurements, including that they can operate at night and during high-latitude winters. This study focuses on the Infrared Atmospheric Sounding Interferometer (IASI). Retrievals developed for this instrument have been shown to be successful when applied to large eruptions, but little has been done to explore their potential for detecting and quantifying emissions from smaller and lower altitude emissions or for the assessment of ongoing activity. Here a "fast" linear retrieval has been applied across the globe to detect volcanic sources of SO_2. The results are dominated by emissions from explosive eruptions, but signals are also evident from weak eruptions, passive degassing, and anthropogenic activity. Ecuador and Kamchatka were selected for further study with a more processing intensive iterative retrieval which can quantify the SO_2 amount. At Tungurahua in Ecuador, good agreement was seen between IASI, the Ozone Monitoring Instrument (OMI) and ground-based flux data, demonstrating that the retrieval is capable of capturing relative changes in activity. Similarly, good agreement was found between IASI and OMI in Kamchatka. In this high-latitude region, OMI is unable to operate for 3 or 4 months in each year. It is therefore suggested that IASI could be used alongside other instruments for evaluating changes in volcanic activity.

Plain Language Summary Gas emissions at volcanoes are dangerous to health and can alter the environment and climate. Monitoring the gases emitted is therefore important, and it gives volcanologists some insight into volcanic behavior. Ground-based monitoring can be dangerous and is limited in remote regions, and so satellite imagery is used to detect and measure volcanic gas emissions (usually sulfur dioxide [SO_2]) across the globe. This study focused on the Infrared Atmospheric Sounding Interferometer, which is an infrared sensor onboard two meteorological satellites. First, a fast tool was used to detect emissions of SO_2 across the globe: including from explosive volcanic activity, smaller eruptions, and human pollution sources. Following this, a second method was applied to calculate the amount of SO_2 emitted from volcanoes in Ecuador and Kamchatka (Eastern Russia)—two regions with regular volcanic activity. This technique was shown to capture changing levels of volcanic activity in both areas. At Tungurahua, a volcano in Ecuador, comparisons could be made to another satellite and to measurements made on the ground. The three methods compared well suggesting that the technique developed for Infrared Atmospheric Sounding Interferometer can capture changing activity at this volcano and could be valuable for tracking and quantifying emissions.

1. Introduction

Geochemical observations provide insight into the magmatic, volcanic, and hydrothermal processes at volcanoes and consequently play a fundamental role in understanding and monitoring their behavior (Edmonds, 2008; Oppenheimer et al., 2014; Scaillet et al., 1998; Symonds et al., 1994). Sulfur dioxide (SO_2) typically comprises only 5% of the total gas emission but as the atmospheric background abundance of the gas is low, and because SO_2 has a distinct spectral signature in both the ultraviolet and infrared regions of the electromagnetic spectrum, the gas has been widely studied (Oppenheimer, 2010; Oppenheimer et al., 2011).

Ground-based UV instruments, such as the correlation spectrometer (COSPEC) (Casadevall et al., 1983; Malinconico, 1979; Moffat & Millán, 1971; Stoiber et al., 1983), and then the smaller miniaturized differential optical absorption spectroscopy (mini-DOAS) (Galle et al., 2003; McGonigle et al., 2002) and Flyspec (Elias et al., 2006; Horton et al., 2006) instruments, have enabled numerous field campaigns and facilitated the installation of automated SO_2 monitoring networks at several volcanoes (e.g., Edmonds et al., 2003; Galle et al., 2003, 2010; McGonigle et al., 2004). However, such field campaigns and instrument networks are expensive and logistically challenging, and so many volcanoes in developing countries and in remote regions have little or no ground-based SO_2 monitoring, and where ground-based measurements are available these are often limited to daytime monitoring and cannot track plumes across large geographic areas.

Satellite technology offers a cost effective solution to some of the limitations of ground-based monitoring and advances over the past few decades mean that it is now possible to monitor many aspects of volcanic behavior from space, including the detection and retrieval of SO_2 emissions from volcanoes across the globe. Volcanic SO_2 was first observed with the Total Ozone Mapping Spectrometer following the eruption of El Chichón in 1982 (Krueger, 1983; Krueger et al., 2008). Since then numerous satellite-based sensors have been used to detect and track SO_2 emissions including the Moderate Resolution Imaging Spectroradiometer (e.g., Corradini et al., 2009, 2010; Novak et al., 2008; Watson et al., 2004), the Advanced Spaceborne Thermal Emission and Reflection Radiometer (e.g., Campion et al., 2010; Pugnaghi et al., 2006; Urai, 2004), the Atmospheric Infrared Sounder (e.g., Carn & Prata, 2010; Carn et al., 2005; Prata & Bernardo, 2007), the Ozone Monitoring Instrument (OMI; e.g., Carn et al., 2008, 2013, 2016, 2017; McCormick et al., 2013; Theys et al., 2013, 2015), the Spinning Enhanced Visible and Infrared Imager (e.g., Corradini et al., 2009; Prata & Kerkmann, 2007; Prata et al., 2007), the Infrared Atmospheric Sounding Interferometer (IASI; e.g., Clarisse et al., 2008, 2012; Carboni et al., 2012, 2016; Walker et al., 2011, 2012), the Global Ozone Monitoring Experiment (GOME-1 and GOME-2; e.g., Eisinger & Burrows, 1998; Rix et al., 2009), and Ozone Mapping and Profiler Suite (e.g., Carn et al., 2015). The higher spatial and spectral resolutions of newer instruments mean it is now possible to detect weaker sources of SO_2, such as smaller eruptive events, noneruptive volcanic degassing and anthropogenic emissions (e.g., Carn, 2016; Fioletov et al., 2015, 2016; Koukouli et al., 2016). Subsequently, measurements of volcanic SO_2 made by satellite instruments have been used in conjunction with ground-based observations to interpret volcanic activity (e.g., McCormick et al., 2013; Rix et al., 2009; Surono et al., 2012).

Within the infrared there are three SO_2 absorption features, ν_1, ν_3 and $\nu_1 + \nu_3$ (centered at 8.7, 7.3, and 4.0 μm respectively), which can be used to obtain information on the gas (Thomas & Watson, 2010). Of these the $\nu_1 + \nu_3$ band is the weakest feature and so it is only used when large quantities of SO_2 cause saturation of the other channels (Karagulian et al., 2010). It is also affected by reflected solar radiation and so this must be accounted for in retrieval techniques (Karagulian et al., 2010). The ν_3 band has been widely used to retrieve SO_2 properties (e.g., Carn et al., 2005; Prata & Bernardo, 2007; Prata et al., 2003). It is the strongest feature, but it is collocated with strong water vapor absorption, which reduces its sensitivity to emissions in the lower part of the troposphere if there are high levels of water vapor. In contrast, the ν_1 feature is situated within an atmospheric window making it the most appropriate method for monitoring emissions into the lower troposphere (Realmuto, 2000; Realmuto et al., 1994, 1997), although it can in turn be affected by volcanic ash and sulfate aerosol (Thomas & Watson, 2010).

IASI is on-board, MetOp A and B, launched in 2006 and 2012, respectively. These advanced Fourier transform spectrometers are coupled with an infrared imager (Blumstein et al., 2004). The two satellites occupy the same orbit with 50 min between them, and both achieve near-global coverage every 12 hr. Each scan has a swath width of 2,200 km composed of circular pixels with a diameter of 12 km at nadir (Clerbaux et al., 2009). One of IASI's main strengths is that it measures across the 645 to 2,760 cm^{-1} (3.62 to 15.5 μm) spectral range with a high spectral resolution of 0.5 cm^{-1} (Blumstein et al., 2004; EUMETSAT, 2017), meaning it is possible to better resolve spectral features. This range incorporates the three previously mentioned SO_2 absorption features, and a number of techniques have been developed to exploit these (e.g., Carboni et al., 2012; Clarisse et al., 2008, 2012; Walker et al., 2012). These retrievals have been successfully applied to a number of different eruptions, summarized in Table 1; however, most of these studies are applications to large explosive eruptions which emit substantial quantities of SO_2 into the atmosphere. In contrast, very little has been done to explore the potential of this instrument for monitoring weaker emissions, such as those from smaller explosive eruptions and noneruptive passive degassing. In this study, a linear retrieval (Walker et al., 2011, 2012) has been used to detect volcanic emissions across the globe, following which an iterative retrieval (Carboni et al., 2012, 2016) has been applied to quantify mass loading of SO_2 in Ecuador and Kamchatka, the aim of this being to

Table 1
Summary of Eruptions Previously Examined With IASI

Volcano	Location	VEI	Start date	Days analyzed with IASI	References	Figure reference
Jebel at Tair	Red Sea,Yemen	3	30 September 2007	12 days	Clarisse et al. (2008)	Figure 1 (2007)
	15.55°N 41.83°E					SM1—frames 1.9 and 1.10
Llaima	Chile	3	2 January 2008	5 days	Carboni et al. (2016)	SM1—frame 2.1
	38.69°S 71.73°W					
Mount Okmok	Aleutian Islands	4	12 July 2008	14 days	Karagulian et al. (2010)	Figure 1 (2008)
	53.43°N 168.13°W				Carboni et al. (2016)	SM1—frame 2.7
Kasatochi	Aleutian Islands	4	7 August 2008	>1 month	Rix et al. (2009)	Figure 1 (2008)
	52.18°N 175.52°W				Karagulian et al. (2010)	SM1—frame 2.8
					Clarisse et al. (2012)	
					Carboni et al. (2016)	
Alu-Dalaffilla	Ethiopia	4	4 November 2008	4 days	Carboni et al. (2016)	Figure 1 (2008)
	13.79°N 40.55°E					SM1—frame 2.11
Sarychev Peak	Kuril Islands	4	11 June 2009	>1 month	Haywood et al. (2010)	Figure 1 (2009)
	48.09°N 153.20°E				Clarisse et al. (2012)	SM1—frame 3.6
					Carboni et al. (2016)	
Soufrière Hills	Montserrat	3	11 February 2010	6 days	Carboni et al. (2016)	Figure 1 (2010)
	16.72°N 62.18°W					SM1—frame 4.2
Eyjafjallajökull	Southern Iceland	4	14 April 2010	>1 month	Carboni et al. (2012)	Figure 1 (2010)
	63.63°N 19.62°W				Heard et al. (2012)	SM1—frames 4.4 and 4.5
					Walker et al. (2012)	
					Boichu et al. (2013)	
Merapi	Java	4	4 November 2010	8 days	Surono et al. (2012)	Figure 1 (2010)
	7.54°S 110.44°E				Carboni et al. (2016)	SM1—frame 4.11
Nyamuragira/	DRC		3 January 2010	10 days	Carboni et al. (2016)	Figure 1 (2011)
Nyiragongo	1.408°N 29.2°E		7 November 2011	9 days		SM1—frames 4.1 and 5.11
Grímsvötn	Northeast Iceland	4	21 May 2011	>2 weeks	Clarisse et al. (2012)	Figure 1 (2011)
	64.42°N 17.33°W				Cooke et al. (2014)	SM1—frame 5.5
					Moxnes et al. (2014)	
					Koukouli et al. (2015)	
					Carboni et al. (2016)	
Puyehue-Cordon	Chile	5	4 June 2011	>1 month	Clarisse et al. (2012)	Figure 1 (2011)
Caulle	40.59°S 72.12°W				Theys et al. (2013)	SM1—frame 5.6
Nabro	Eritrea	4	12 June 2011	18 days	Carboni et al. (2016)	Figure 1 (2011)
	13.37°N 41.70°E				Clarisse et al. (2014)	SM1—frames 5.6 and 5.7
Copahue	Chile-Argentina	2	22 December 2012	6 days	Carboni et al. (2016)	Figure 1s (2012)
	37.85°S 71.18°W					SM1—frame 6.12
Etna	Italy		Multiple eruptions		Carboni et al. (2016)	e.g., SM1—frames 2.5, 6.1,
	37.75°N 14.99°E					7.10, and 7.11

Note. IASI = Infrared Atmospheric Sounding Interferometer. VEI = Volcanic Explosivity Index.

demonstrate, for the first time, that there is some utility for using these retrievals to capture long-term changes in volcanic activity.

2. Linear Retrieval

2.1. The Algorithm

The "fast" linear retrieval developed by Walker et al. (2011, 2012) works by separating the signal of the target species (SO_2) from that of the spectral background. To do this, a covariance matrix is formed from an ensemble of SO_2 free pixels which represent variability in the spectra due to the parameters which are not being

retrieved. The spectra of pixels containing SO_2 deviate from this background so allowing them to be quickly distinguished. The speed of this technique facilitates its use for scanning large data sets in near real time; for example, for hazard assessments or for the identification of sites for further study. But by using the full spectra in either the ν_1 or ν_3 absorption bands (in this study the ν_3 was used), it has been shown to be more sensitive to the presence of SO_2 than techniques developed for IASI which only use a small selection of channels (Walker et al., 2011, 2012). The detection limit of this technique ranges from 0.3 DU at altitudes of 14 to 18 km, to 17.0 DU close to the surface (0–2 km), or 1.3 DU at between 4 and 6 km, more similar to the height of volcanic plumes from smaller or noneruptive activity (Walker et al., 2012).

The output of the linear retrieval is an "effective" SO_2 column amount under the assumption of a standard atmospheric profile and that the SO_2 profile that has a uniform distribution between 0 and 20 km. It is used here as a tool to flag volcanic emissions, following which the Carboni et al. (2012) iterative retrieval can be used to fully quantify the amount of gas. As with previous studies using this technique (Walker et al., 2011, 2012), the covariance matrix used is formed from pixels over the North Atlantic and Europe in May 2009. This can produce systematic errors in areas with notably different climatologies.

2.2. Linear Retrieval Results

To enhance the SO_2 signal, and particularly to emphasize smaller emissions, the linear retrieval output has been gridded to a 0.125° latitude by 0.125° longitude grid and averaged for each year studied. This includes both the morning and evening overpasses and does not filter for cloud. The results are shown in Figure 1. Alongside this, monthly average results are displayed in Movie S1 in the supporting information (SM1) and are referred to by their frame number. These plots provide a snapshot of activity within the represented time frame; a function of numerous factors such as the quantity of SO_2 emitted, the rate of SO_2 decay and transportation, and the atmospheric state at the time of the instrument overpass.

2.2.1. Volcanic Emissions Across the Globe

The linear retrieval yearly averages, shown in Figure 1, are largely dominated by emissions from major eruptions during each year, most notably Kasatochi, Sarychev Peak and Nabro in 2008, 2009, and 2011, respectively. Most of the SO_2 emissions previously explored with IASI (listed in Table 1) can be identified within the yearly averages, and all can be identified in the monthly averages shown in SM1.

Smaller signals can also be identified in the global yearly and monthly averages. For example, elevated signals can be regularly identified at Popocatépetl, which is one of Mexico's most active volcanoes (Delgado Granados & Cardenas Gonzalez, 2013; Grutter et al., 2008). Other examples of plumes from effusive activity are Fernandina in the Galapagos in April 2009 (frame 3.4) and at Pico do Fogo in Cape Verde in November 2014 (frame 8.11). Emissions from low-level activity or passive degassing can also be commonly identified across the Central and South American volcanic arcs, in Kamchatka and in Indonesia, the Philippines, Papua New Guinea, and Vanuatu. These, and other, lower level emissions can be seen more clearly in regional plots, and Central and South America and Kamchatka are explored in the following section.

2.2.2. Regional Volcanic Emissions

Central and South America, and Kamchatka (Eastern Russia), are two volcanic arcs where emissions are frequently identified with the linear retrieval. Expanded views over these regions are presented in Figure 2. These offer more detail on the activity occurring within these regions. In this figure, (a) and (c) are yearly averages computed for the regions, and (b) and (d) show monthly averages for each region, displayed with a color bar that ranges from 1 standard deviation below the mean to 3 standard deviations above it, computed separately for each region and month.

Figures 2a and 2b show the expanded view over Central and South America for 2008. In both the yearly and monthly averages, low SO_2 column amounts can commonly be seen off the west coast of Colombia, Ecuador and Peru and sometimes over the landmass as well. Some of this might be from low levels of SO_2, but in many cases this is likely to be due to parameters not fully represented within the covariance matrix. However, despite this elevated levels of volcanic SO_2 can be easily identified. As noted in the previous section, Popocatépetl is the strongest and most persistent source in the region and can be clearly identified in each of the monthly averages shown in Figure 2b. From April 2008, emissions can be easily seen at Nevado del Huila in Colombia, which was active throughout 2008 (Global Volcanism Program [GVP], 2012a). Signals are also commonly seen at Tungurahua in Ecuador (e.g., January–May and December 2008). Alongside this, elevated levels of SO_2 can be identified in Northern Ecuador in November 2008 which is likely to be from eruptions at Reventador (GVP, 2009). Further emissions can be seen in Peru and Chile. In the south of Peru this is coincident with the

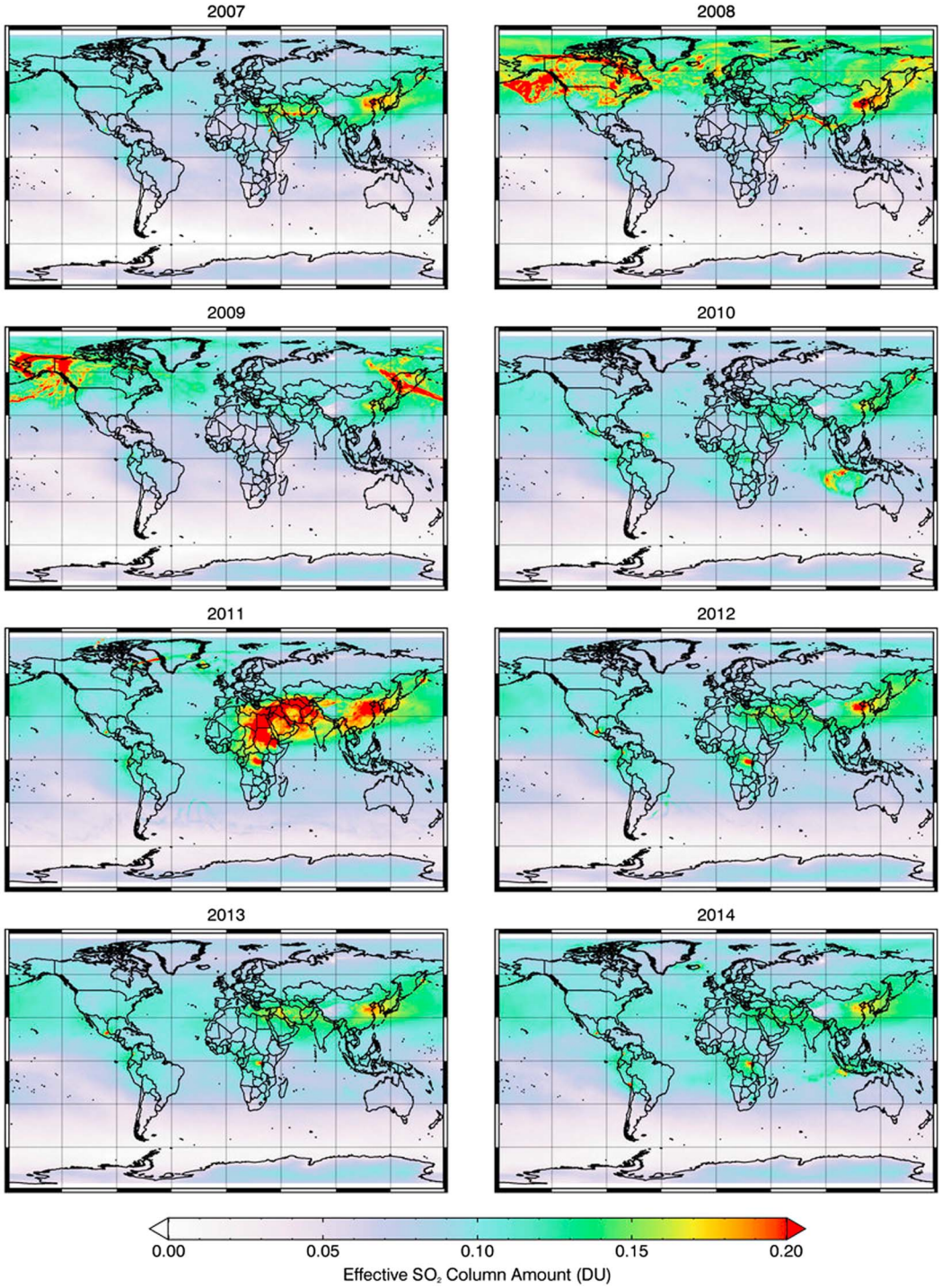

Figure 1. Global averages of the linear retrieval "effective" SO_2 column amounts for the years 2007 to 2014. Emissions from large eruptions can be identified in each year, along with emissions from persistently degassing volcanoes and emissions from anthropogenic sources. Slightly elevated values over Antarctica are attributed to the extreme in climate here with respect to the covariance matrix applied. Low levels of SO_2 are also apparent over the ocean. In some cases, this might be related to volcanic or anthropogenic emissions. For example, higher values over the Pacific Ocean east of China may be due to drifting pollution. In some cases, however, this maybe an artifact of the retrieval.

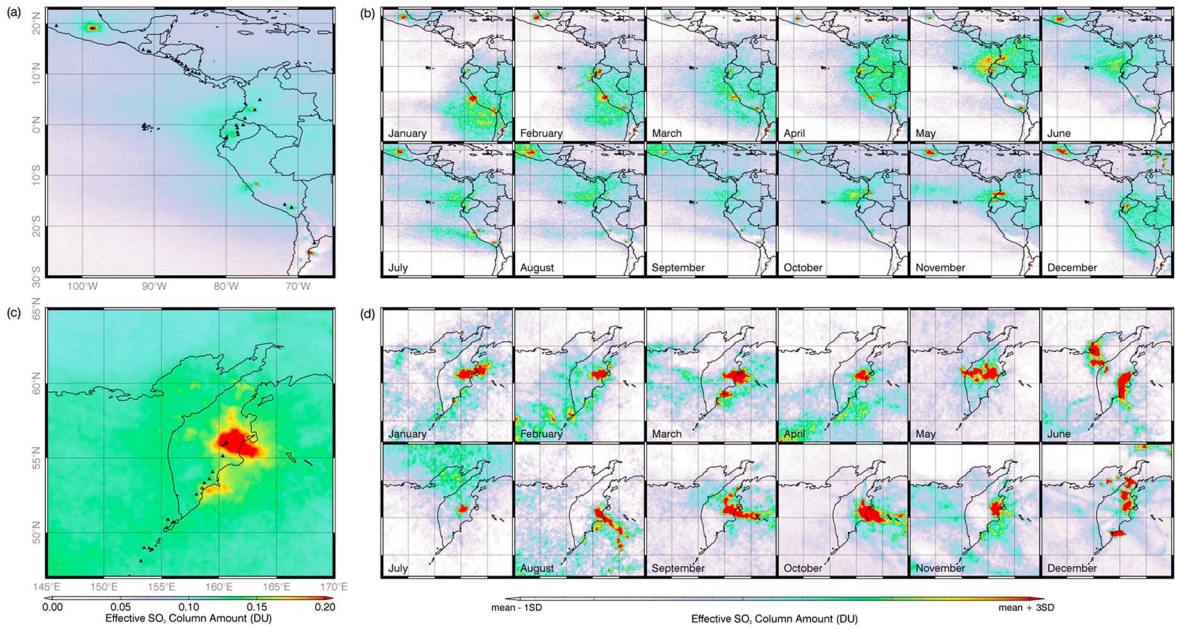

Figure 2. Regional linear retrieval output. (a) The 2008 yearly average effective SO_2 column amounts over Central and South America. (b) Monthly average effective SO_2 column amounts over Central and South America in 2008. These are displayed with a color bar that ranges between 1 standard deviation below the mean to 3 standard deviations above it. These values have been computed for the region and each month separately. This helps emphasize SO_2 sources in the region. (c) The 2010 yearly average effective SO_2 column amounts at Kamchatka. Note that there are relatively high background values across the region. This is potentially linked to pollution from China which is blown northeast with prevailing winds. (d) as (b) for Kamchatka in 2010.

volcano Ubinas that was actively erupting or degassing throughout the year (Rivera et al., 2010). In 2008, there is also commonly a signal over Lascar in Chile, and while there were no GVP reports of volcanic activity at the volcano in this year, the volcano is known to be a persistent passive source of SO_2 (Menard et al., 2014). The use of this retrieval could therefore be valuable for assessing increased levels of volcanic activity. In both Peru and Chile, the source of elevated emissions can be somewhat ambiguous due to numerous copper smelting sites in the region. In Central Peru, where there are no known active volcanoes, a strong and persistent plume of SO_2 can be identified in each month in 2008. This is consistent with the location of the La Oroya multimetal smelter which was studied with OMI in Carn et al. (2007), who demonstrated that it emitted roughly 0.07 ± 0.03 Tg annually in 2004 and 2005.

The Kamchatka region in Eastern Russia is displayed in Figures 2c and 2d for 2010. The volcanoes in this region are remote and have little ground-based monitoring; consequently, satellite remote sensing has been widely employed here to monitor the risk to aviation (Dean & Dehn, 2015). In this region, high background levels in the yearly average may be associated with pollution transported northeast from China. Volcanic SO_2 emissions are seen across the arc, but the high number of active volcanoes in close proximity makes it difficult to accurately discern the origin without information from other sources. In the monthly averages, it is possible to see emissions in the northern part of the Kamchatka region, originating from Klyuchevskoy, which was actively erupting throughout 2010 (GVP, 2010a, 2013a). Shiveluch was also active during this period (GVP, 2010b, 2010c) and may be a contributor to the plumes seen. Elevated signals can also be observed toward the south of the Kamchatka peninsula (e.g., in March and December) and can be attributed to activity at Karymsky volcano, which experienced vulcanian and strombolian eruptions throughout 2010 (Neal et al., 2014).

2.2.3. Anthropogenic Emissions

As already noted it is possible to detect SO_2 emissions from anthropogenic sources with IASI. Numerous studies have been conducted looking at these emissions with OMI (e.g., Carn et al., 2007; Fioletov et al., 2013, 2016, Krotkov et al., 2016), but to date, there have been relatively few studies undertaken with IASI (Bauduin et al., 2014, 2016). In Figure 1 and SM1, a number of different anthropogenic sources can be identified. The easiest to identify is pollution from China which has a prominent signal across the northeastern coast of the country. Despite air quality policies, China remains the largest emitter of SO_2; responsible for roughly 30% of global emissions in 2010 with the majority of this resulting from coal burning (Klimont et al., 2013). Two elevated peaks can also be observed in Iran (clearest in 2012 and 2013, or in the monthly averages—frames 2.3,

4.11, and 5.4), which are in the proximity of the Isfahan heavy oil fired power plant and Sarcheshmeh copper complex also identified in Fioletov et al. (2013, 2016). Another spike of SO_2 is present close to Johannesburg in South Africa (e.g., frames 1.9, 4.9, 5.9, and 8.7), the result of a cluster of power plants burning fossil fuels (Fioletov et al., 2016). Given the relatively sparse availability of literature on using IASI to detect anthropogenic emissions, these areas could be selected for further study in the future.

3. Iterative Retrieval

Emissions were commonly identified with the linear retrieval in Ecuador and Kamchatka and were selected for further study with the iterative retrieval to quantify SO_2 emissions from volcanic activity at the two arcs. Additional reasons for the selection of these two regions are given below.

3.1. The Algorithm

The spectra measured by IASI are a function of a number of atmospheric constituents such as meteorological cloud, H_2O, CO_2, CO, O_3, N_2O, CH_4, and SO_2, each with different concentrations and vertical atmospheric distributions, alongside additional variations caused by temperature, atmospheric pressure, and instrument viewing geometries. The problem of retrieving SO_2 can be simplified by representing the spectral variability generated by other parameters within a covariance matrix, allowing SO_2 to be independently retrieved (Carboni et al., 2012). In this study, the global covariance matrix from Carboni et al. (2016) has been used. The Carboni et al. (2012) iterative retrieval uses European Center for Medium-Range Weather Forecasts data (including temperature and water vapor vertical profiles) within the fast radiative transfer model RTTOV with the addition of SO_2 coefficients, to forward model a clear (i.e., free of meteorological cloud) IASI atmospheric spectra. A range of SO_2 plumes are simulated for the established clear-sky atmosphere, for the entire ν_1 and ν_3 bands. The modeled spectra that best match the observed spectra, determined with a cost function, are taken as the SO_2 column amount and altitude solution, together with the surface temperature (Carboni et al., 2012). In this case, where the iterative retrieval is being applied to pixels containing low concentrations of SO_2 from small explosive eruptions or degassing, there is not enough information within the IASI spectra to obtain both the SO_2 altitude and column amount, and therefore, the plume altitude has been set at 500 mb (~5,600 m), based on the height of volcanoes in the regions studied, Table 2, as is done for many other satellite instruments (e.g., Carn et al., 2013). Note that the true plume height will vary between different volcanoes, different styles of activity, and during eruptions as the cloud disperses and if the true altitude of the plume is lower than the assumed value, then the SO_2 column amount will be underestimated, and vice versa.

One of the advantages of this technique is that it generates a comprehensive error matrix which represents the discrepancy between the modeled and observed spectra in scenes free of SO_2, thereby incorporating forward model and forward model parameter errors, and providing quality control and comprehensive error estimates of the retrieved state. The detection limit of the iterative retrieval is strongly dependent on the altitude of the SO_2 plume and the temperature contrast between the surface and the atmospheric temperature at the plume layer. It can therefore range from around 10.5 DU at the surface to 0.1 DU at the tropopause. Typically, at 3 km the detection limit is around 1 DU. Given this, greater errors are usually associated with small, low-altitude plumes. Error analysis conducted by Carboni et al. (2012) has also demonstrated that thick meteorological cloud or ash above the plume can affect the signal obtained by the instrument and therefore cause the SO_2 column amount to be underestimated. For example, an ash layer with an optical depth of 2 would cause the SO_2 amount to be underestimated by around 50% and an ash layer with an optical depth of 5 would mask the SO_2 entirely. Meteorological cloud has a similar effect. In both cases, this would be distinguishable in the cost function which would increase.

3.2. Ecuador and South Colombia

3.2.1. Background

There are a number of active volcanoes in both Ecuador and Colombia, and these are monitored by the Instituto Geofísico of Escuela Politécnica Nacional and the Servico Geológico Colombiano, respectively. At Tungurahua, in Ecuador, this includes measurements of gas emissions made by a DOAS network (Hidalgo et al., 2015). A summary of ground-based SO_2 flux measurements for volcanoes in the region is reported in Table 2. The availability of this ground-based data set and previous satellite studies of volcanic emissions of SO_2 in the region (Carn et al., 2008; McCormick et al., 2014) make this an appropriate region to begin assessing the strengths and limitations of the Carboni et al. (2012) iterative retrieval. In this study, the iterative retrieval has been applied between June 2007 and December 2013, over a region which includes five active volcanoes: Reventador, Guagua Pichincha, Tungurahua and Sangay in Ecuador, and Galeras in Southern Colombia.

Table 2
Published Ground-Based Estimates of SO_2 Emissions at Active Volcanoes in Ecuador, South Colombia, and Kamchatka

Region	Volcano	Coordinates	Altitude (m)	Average SO_2 flux (tday^{-1})	Method used	Years	Reference
Ecuador/Colombia	Galeras	1.22°N 77.37°W	4,276	~200	COSPEC	1992–1993	Fischer et al. (1994)
				~500	DOAS	2012–2013	Global Volcanism Program (GVP, 2013b)
	Reventador	0.08°S 77.66°W	3,562	1,000	DOAS	2009	GVP (2009)
	Guagua Pichincha	0.17°S 78.60°W	4,784	170 (max)	COSPEC	1998	GVP (1999)
	Tungurahua	1.47°S 78.44°W	5,023	1,458	COSPEC/DOAS	1999–2008	Arellano et al. (2008)
				948	DOAS	2008–2013	Hidalgo et al. (2015)
	Sangay[a]	2.01°S 78.34°W	5,300	—	—	—	
Kamchatka	Shiveluch	56.65°N 161.36°E	3,307	>500	Visual estimate[b]	—	Taran (2009)
	Klyuchevskoy	56.06°N 160.64°E	4,750	>300	Visual Estimate[b]	—	Taran (2009)
	Bezymianny	55.97°N 160.6°E	2,882	400	FLYSPEC	2007	Clark et al. (2007)
	Tolbachik	55.83°N 160.33°E	3,682	~1,500–2,200	DOAS	2013	Melnikov et al. (2014)
	Kizimen	55.13°N 160.32°E	2,376	700	DOAS	2012	Melnikov et al. (2014)
	Karymsky	54.05°N 159.44°E	1,345	432	DOAS	2011	Arellano et al. (2012)
				60–121	FLYSPEC	2011–2012	Lopez et al. (2013)
				350–400	DOAS	2012–2013	Melnikov et al. (2014)
	Zhupanovsky	53.59°N 159.15°E	2,958	>100	Temperature estimate[c]	—	Taran (2009)
	Koryaksky	53.32°N 158.71°E	3,456	>20	Temperature estimate[c]	—	Taran (2009)
	Avachinsky	53.26°N 158.84°E	2,741	210	DOAS	2012–2013	Melnikov et al. (2014)
	Gorely	52.56°N 158.03 °E	1,829	800–1,200	DOAS	2012–2013	Melnikov et al. (2014)
				800	Dual-UV Camera	2011–2012	Aiuppa et al. (2012)
	Mutnovsky	52.45°N 158.2°E	2,322	480	DOAS	2012–2013	Melnikov et al. (2014)

[a]No reports on SO_2 flux available at Sangay. [b]Based on the frequency and size of the eruptive plume compared to volcanoes elsewhere in the world where SO_2 flux is recorded. [c]Estimated by measuring temperatures of escaping gas and using thermodynamic mass balances.

3.2.2. Negative Bias Characteristics and Correction

Following the application of the iterative retrieval over Ecuador, persistent negative values of up to −0.4 DU were observed (e.g., Figure 3c). This has not been noted in previous applications of this algorithm, and while some, near zero, background fluctuations might be expected due to instrument noise, an offset of this magnitude implies that other factors are influencing the result. As seen in Figure 3, the bulk of the negative values is situated to the north of Ecuador, consistent with mountainous terrain to the north of the country.

One of the possible explanations for this is the covariance matrix used within the retrieval. As in Carboni et al. (2012, 2016) a covariance matrix consisting of more than 5 million SO_2 free pixels from across the globe, and from four seasons in 2009, was used. This global matrix could under represent the variability in the environment, climate, and surface conditions in this region; for example, surface emissivity in the region varies significantly from tropical rainforest to rocky mountainous terrain. In an attempt to improve this, local emissivity values from the Cooperative Institute for Meteorological Satellite Studies Infrared Emissivity Database have been incorporated into the RTTOV model, leading to a reduction of the bias by 20–30%. However, a significant offset remains.

Ideally, new localized covariance matrices would have been formed; however, this process is not straightforward. A large number of pixels are required to represent background variability in the covariance matrix; however, these must be free of SO_2. In both regions studied there are continuously degassing volcanoes and frequent eruptions, making it difficult to select appropriate pixels. This is further complicated in Kamchatka (discussed in more detail in section 3.3.2) where SO_2 has been carried into the region from other eruptions (e.g., Kasatochi and Sarychev Peak, SM1—frames 2.8 and 3.6) and from pollution in China.

Previous studies have corrected for negative values by adjusting the output using an area free from SO_2 (Carn et al., 2008; McCormick et al., 2014). In this case, the spatial variability of the negative values, coupled

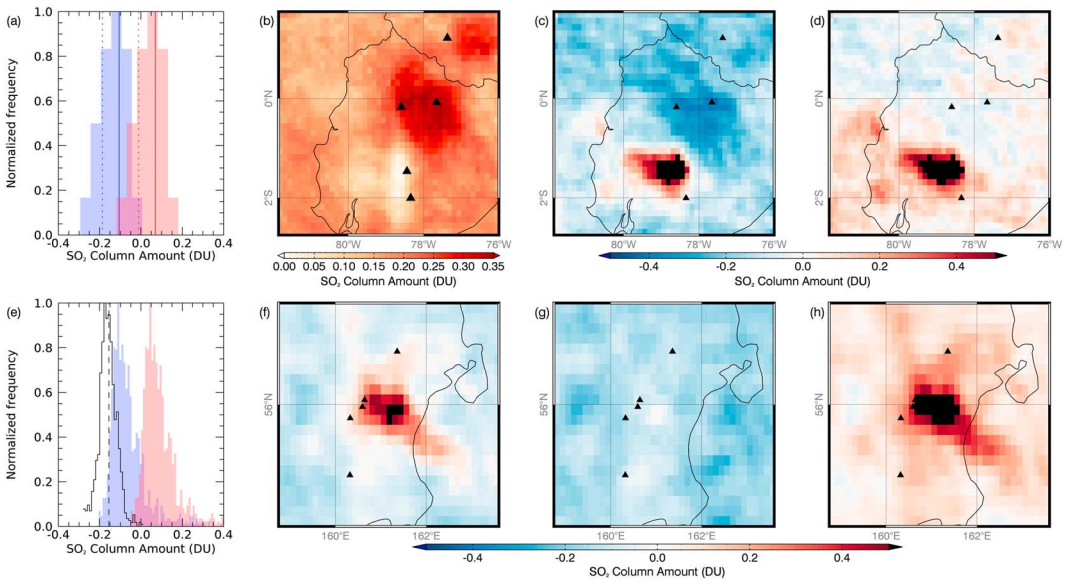

Figure 3. Bias correction over Ecuador and Kamchatka. (a) Distribution of the uncorrected (blue) and corrected (red) monthly average SO_2 column amounts for a single grid box in the Ecuador region. Solid line shows the mean and the dashed line shows 1 standard deviation from the mean. The lowest value, for each grid box, which fell within 1 standard deviation of the mean was used to correct the average column amount. (b) The correction applied over the Ecuador region for the June 2007 to May 2010 time period. (c) Uncorrected monthly average SO_2 column values over Ecuador in January 2010. (d) Corrected values for January 2010. (e) Distribution of SO_2 column amounts in the northern Kamchatka region for September 2010. The uncorrected values are shown in blue and the distribution of uncorrected values following the removal of pixels flagged as containing SO2 is shown in black. The dashed black line is the average of the uncorrected grid boxes after pixels which contain SO_2 have been removed. This is used to correct the bias. The distribution of corrected values is shown in red. (f) Uncorrected monthly average SO_2 column amount for September 2010. (g) Uncorrected monthly average SO_2 column amount for September 2010 excluding pixels that contained SO_2. (h) Corrected values for September 2010.

with the close proximity of volcanoes emitting varying degrees of SO_2 (making it difficult to determine which boxes are truly SO_2 free), makes this method inappropriate. Instead, the following steps were implemented to remove the majority of the bias: (1) data were gridded into 0.125° by 0.125° grid boxes and averaged for each month (incorporating both morning and evening overpasses). (2) For each grid box the average and standard deviation of the SO_2 column amount were computed for the periods before and after May 2010, during which there was a calibration change to the instrument which caused a jump in the magnitude of the bias. (3) The lowest value, for each grid box, which fell within 1 standard deviation of the mean was used to correct the total column amount. Figure 3b shows how this correction value, for the pre May 2010 period, changes across the region. This removes the majority of the bias as can be seen in Figures 3c and 3d, which show the average SO_2 column amount in January 2010 before and after the correction has been applied. However, it is possible that the correction may be underestimated in some cases. For example, as seen in Figure 3b, the correction applied varies significantly across the region and west of Tungurahua and Sangay; the correction is close to zero. It is possible that these areas are simply bias free; however, it is also possible that this is a consequence of higher levels of SO_2 in the region meaning that no negative values were produced, and so the bias correction may be underestimated. Nonetheless, this technique removes the majority of the bias from the region allowing interpretation of changing quantities of SO_2.

3.2.3. Arc-Scale Observations

The iterative retrieval was run over Ecuador and the south of Colombia from June 2007 to December 2013. Maps of the monthly average SO_2 column amounts are presented in Figure S1 in the supporting information. These show that throughout the time period explored, Tungurahua dominates emissions across the arc. Emissions, however, are also observed from Reventador and Galeras.

A small selection of the iterative retrieval monthly averages is presented in Figure 4 alongside the monthly average output from a DOAS retrieval developed for OMI by Theys et al. (2015). Note that this procedure assumes an altitude of 7 km, more similar to the height of plumes from explosive activity in the region. This

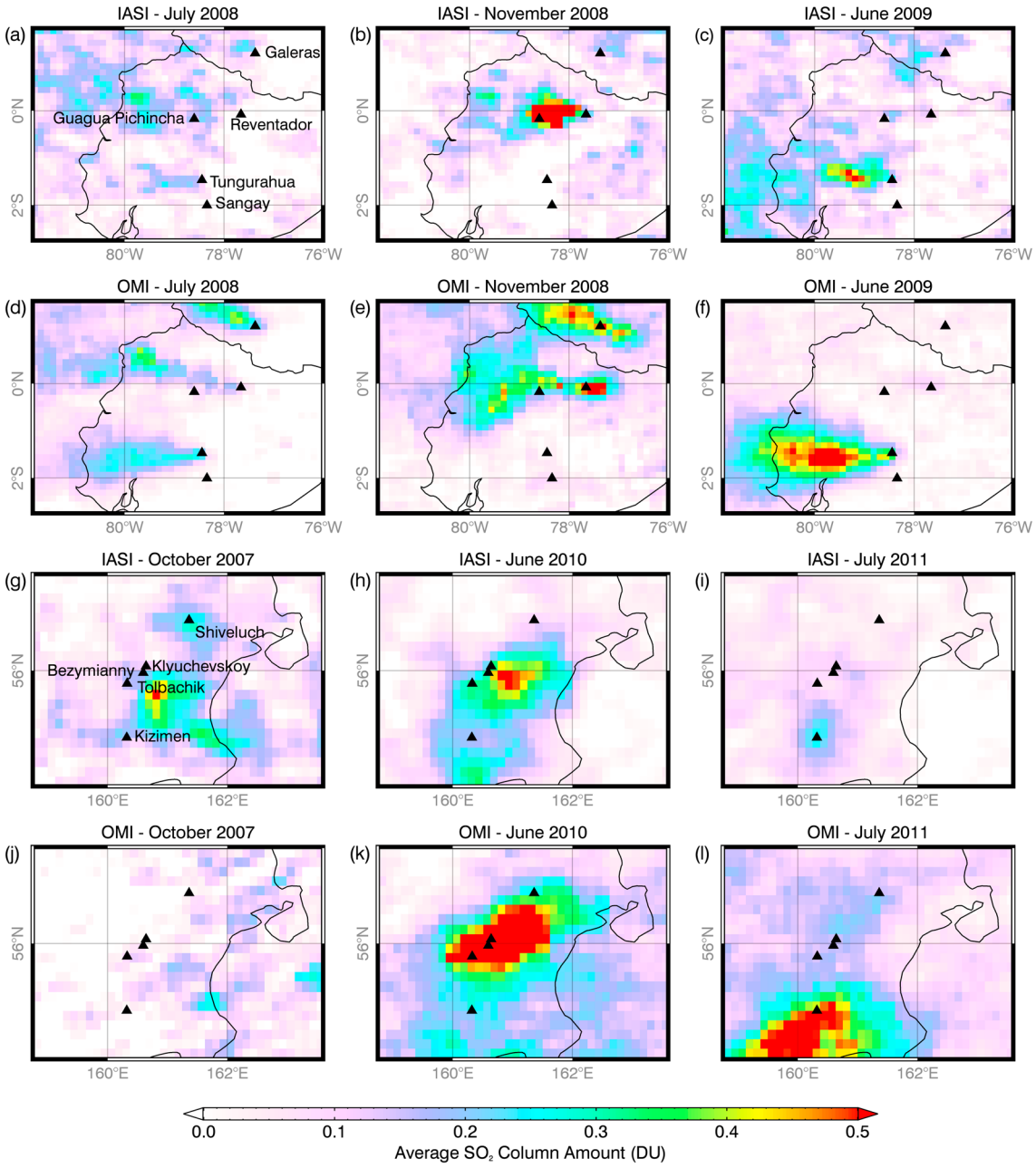

Figure 4. Maps of monthly average SO_2 column amounts from the Infrared Atmospheric Sounding Interferometer (IASI) and Ozone Monitoring Instrument (OMI) retrievals over Ecuador and Kamchatka.

could result in a difference of 15% compared to if the retrieval had been run using the same plume height assumed in the IASI retrieval (roughly 5.6 km).

Figure 4 shows that plumes identified with the OMI DOAS procedure are larger and more defined than those seen with IASI. For example, three substantial plumes can be seen in Figure 4d, but in the IASI monthly averages the plumes are not so clearly defined. Similarly, in November 2008, plumes can be seen at Reventador and Galeras in Figure 4e but only at Reventador with IASI. Also, a much larger plume is seen at Tungurahua in Figure 4f than in Figure 4c. There are a number of possible explanations for these results. First, the altitude assumed in the iterative retrieval is based on typical emission heights at Tungurahua, the second highest and the most active volcano in the region. By comparison Galeras and Reventador are over 700 m lower and so it follows that the plume altitude would also be lower. Therefore, potentially, this may lead to the underestimation of the SO_2 column amounts. Ultraviolet measurements by comparison are less sensitive to the assumed

Table 3
Summary of Activity at Tungurahua Between 2007 and 2013

Period	Phase	Start	End	Average height above crater (km)	Number of explosions	Average daily SO_2 flux (tonnes)	Activity description
1	I	24/02/2007	04/08/2008	2.7	1,763	674 ± 667	Near continuous activity with paroxysm in February 2008, followed by a drop in activity
2	II	16/12/2008	01/03/2009	2.6	377	1,675 ± 1,229	Six short episodes of strombolian activity
	III	28/03/2009		2.3	212	934 ± 694	
	IV	30/12/2009		2.5	521	1807 ± 1394	
	V	26/05/2010	03/08/2010	2.9	1351	1466 ± 1358	
	VI	22/11/2010	03/01/2011	2.7	111	1169 ± 1176	
	VII	20/04/2011	26/05/2011	3.5	64	1661 ± 1505	
3	-	27/11/2011	09/04/2012	3.3	194	826 ± 1289	Near continuous activity with sharp spike at the onset
4	VIII	14/12/2012	10/01/2013	2.8	453	1241 ± 1051	Four phases of strombolian activity
	IX	01/03/2013	17/03/2013	2.2	118	1186 ± 787	
	X	27/04/2013	16/05/2013	2.0	151	1872 ± 1637	
	XI	14/07/2013	05/08/2013	3.8	64	1430 ± 929	

Note. Modified from Hidalgo et al. (2015). The SO_2 flux is given for each time period and phase and also shows the variability in the data- standard deviation from the averages.

altitude. As IASI is an infrared instrument it is also limited in the lower part of the troposphere by the temperature contrast between the Earth's surface and the air above it so lowering the sensitivity of the instrument (Bauduin et al., 2014; Deeter et al., 2007). The iterative retrieval also has a higher detection limit than the OMI retrieval in the lower parts of the troposphere, at roughly 1 DU at 3 km. In contrast, the detection limit for the OMI retrieval is much lower at around 0.5–0.6 DU in the boundary layer and 0.25–0.3 DU at the assumed retrieval height. Additional variations may also arise from differences in SO_2 and in atmospheric conditions in the different overpasses. While in general clearer stronger plumes can be seen with OMI, in June 2009, a faint plume can be seen at Galeras with the IASI technique, but this is nonexistent in the OMI output. This corresponds to a period of elevated activity including increased gas and ash emissions (GVP, 2009).

3.2.4. Activity at Tungurahua

As shown in Figure S1, Tungurahua is the most active volcano in the studied region, and regular monitoring at the volcano means that activity here is well constrained. Monitoring efforts include gas measurements made by a DOAS network setup in 2007. A synthesis of these results was produced by Hidalgo et al. (2015), and using these measurements, activity at the volcano between 2007 and 2013 was divided into four periods, summarized in Table 3. Average total masses of SO_2 at Tungurahua were calculated from the monthly average SO_2 column amounts, shown in Figure S1 in the supporting information, using the area shown in the map in Figure 5a. The results, Figure 5a, demonstrate that there is generally good agreement here between the OMI and IASI results and that these match periods of activity at the volcano (shaded in gray). One notable difference in the time series for the two instruments is in April 2011. During this month there was explosive activity with plumes exceeding the assumed height of 5.6 km which may have led to overestimation of the IASI average total SO_2 mass. Average total SO_2 masses obtained with the IASI iterative retrieval and OMI DOAS procedure have a high correlation coefficient of 0.91 for June 2007 to May 2010. Following this, there was a change to IASI's calibration, resulting in a generally higher total average SO_2 mass relative to OMI, which rarely returns to zero during periods of quiescence. Despite this, the correlation coefficient remains relatively high at 0.87 for the remainder of the study period, implying that both instruments are faithfully recording prevailing activity. It is important to note that the average total amount of SO_2 reported in Figure 5a at Tungurahua is computed for a small region shown in the map in Figure 5a, which is where SO_2 is typically seen with the IASI iterative retrieval, and the same area is used for the OMI data for comparison. However, as seen in Figure 4, the plumes as seen with OMI are much larger and so these values are not a true representation of the absolute magnitude of SO_2. Using an area more reflective of the plumes seen with OMI sees a drop in the correlation coefficient to 0.48 and 0.76 before and after May 2010, respectively. A change in the gradient of the regression line describing the relationship between the two is also noted, with a fall from 1.08 to 0.8 in the first period,

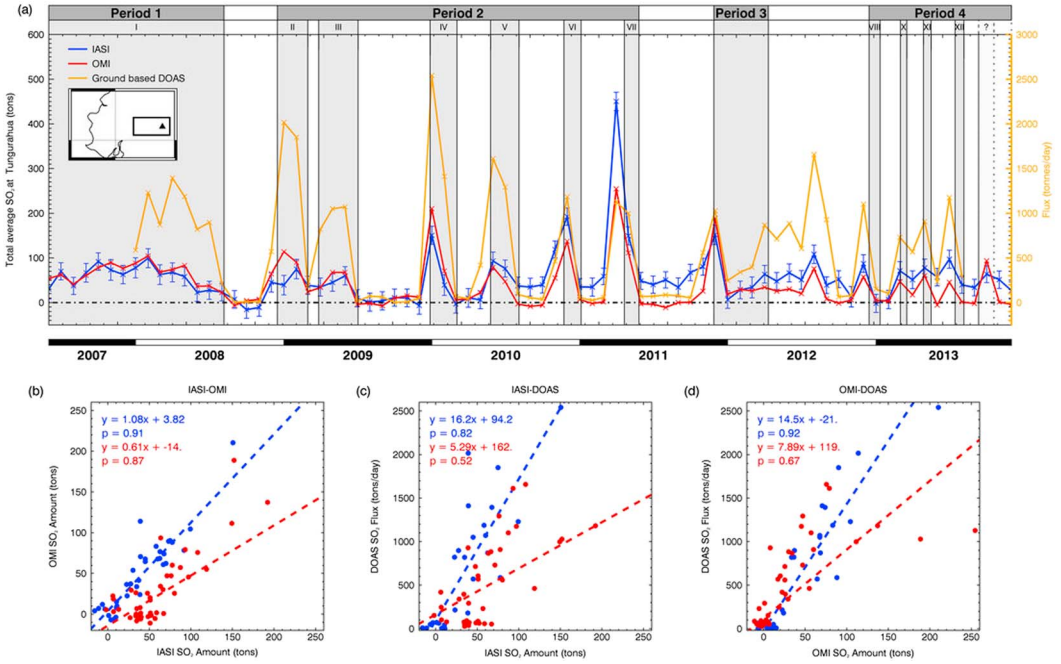

Figure 5. (a) Time series of total monthly average of SO_2 around Tungurahua from the Infrared Atmospheric Sounding Interferometer (IASI) and the Ozone Monitoring Instrument (OMI) for June 2007 to December 2013, and the monthly average SO_2 flux recorded with a DOAS network and published in Hidalgo et al. (2015). Average total masses of SO_2 at Tungurahua were calculated from the monthly SO_2 column amounts using the box area shown in the map. Shaded in gray are episodes of activity noted in the Hidalgo et al. (2015) paper, described in Table 3. The error bars on the IASI average total SO_2 masses incorporate the instrumental error, and errors associated with the forward model, meteorological data and nonperfect representation of gas absorption and errors due to the presence of cloud. (b) Comparison of IASI and OMI total monthly averages of SO_2 amounts at Tungurahua. Shown in red are the equation of the line describing the relationship and correlation coefficients for the period before May 2010 and in blue the same for the period after May 2010. (c) Same as (b) for IASI and ground-based flux measurements averaged for each month. (d) Same as (b) for OMI and ground-based DOAS measurements.

and an increase from 0.61 to 0.75 in the second. Nevertheless, it is clear that both instruments are capable of detecting relative changes in volcanic activity and that these match the periods of activity as noted in Hidalgo et al. (2015).

The average total mass values have also been compared against the ground-based SO_2 flux measurements made by the DOAS network, shown in Figure 5a. It is important to emphasize that these flux measurements are distinct from those made by the satellite instruments. The former is a flux (tonnes per day) obtained by continuous measurements throughout daylight hours and averaged for each month, while the second is a measure of the total SO_2 in tons across a wider region obtained through daily (OMI) or twice daily (IASI) measurements averaged for each month. The flux measure is also a function of wind speed. While these measurements are not directly equivalent, they should in principle be correlated, and as shown in Figure 5a this is generally the case. High correlation coefficients of 0.92 and 0.67 were computed for the OMI-DOAS instrument combination for the periods January 2008 to May 2010, and May 2010 to August 2013. Fairly high values, 0.82 and 0.52, were also recorded for the IASI-DOAS combination. If a steady state of emissions and an SO_2 lifetime of one day were assumed at Tungurahua it would be expected that the average total SO_2 mass would be equivalent to the monthly average flux (McCormick et al., 2014). However, this is not the case with an order of magnitude difference between the average total SO_2 mass obtained with the satellite retrievals and the average flux. In this case, however, the area used to calculate the total monthly average SO_2 mass at Tungurahua does not always represent the full extent of the plume and this may be one reason why the total SO_2 mass is lower than the emission rate. Given this, a closer match between the monthly average total SO_2 mass obtained with OMI and IASI and the average flux from the ground-based DOAS is obtained if a wider area around Tungurahua is considered. This is more reflective of the larger plumes seen with OMI. Additional variations may arise from high plume transport speeds that carry the gas away from the vent and the area being used to calculate the SO_2 mass, and SO_2 depletion and dissipation away from the source leading to it being no longer detectable by

the satellite instruments. It is also possible that in Ecuador's tropical climate, the lifetime of SO_2 in the region is less than 1 day as is discussed in McCormick et al. (2014). Nonetheless, looking beyond the absolute values, these results suggest that the IASI (and OMI) retrievals are able to convincingly detect relative changes in volcanic activity. The published flux data cease in August 2013, but following this, there is an additional rise and fall in October 2013, implying an additional episode of strombolian activity in period 4. This is supported by GVP reports that note an increase in activity with elevated levels of seismicity, increased strombolian explosions, and ash emissions beginning on the 6 October 2013 (GVP, 2013c) and continuing throughout the month with a maximum SO_2 flux of 725 tons per day in the last week of October (GVP, 2013d). Activity remained high in November, primarily characterized by ash clouds, some rising a few kilometers above the vent (GVP, 2013e), before activity subsided midway through the month.

3.3. Kamchatka

3.3.1. Background

There are numerous, remote volcanoes on the Kamchatka peninsula and nearby Kuril Islands, and these pose a significant hazard to the high volume of aircraft which pass over or near to the region (Dean & Dehn, 2015). Their remote nature means that monitoring efforts are highly dependent on satellite remote sensing. Despite significant degassing across the arc, Kamchatka has previously been poorly represented in global volcanic SO_2 budgets (Andres & Kasgnoc, 1998; Halmer et al., 2002) and field campaigns such as Arellano et al. (2012) and Melnikov et al. (2014; results summarized in Table 2) only represent a snapshot of ongoing activity. Using UV satellite sensors, the latest global volcanic SO_2 budget better represents volcanic SO_2 emissions from Kamchatka (Carn et al., 2017). However, these instruments are limited by the loss of sunlight hours in winter (McCormick et al., 2013), meaning there is a potential advantage to using infrared sensors like IASI. Here the IASI iterative retrieval is run over the northern Kamchatka region for a 7-year period during which activity was reported at five volcanoes: Shiveluch, Klyuchevskoy, Bezymianny, Tolbachik, and Kizimen.

3.3.2. Bias Characteristics and Correction

As with Ecuador, negative SO_2 column amounts can be observed over the northern Kamchatka region. Here there is no strong geographic trend but there is significant seasonal variation, with the bias being more extensive during the summer and autumn (May–September). This seasonality suggests that surface components such as surface temperature, moisture changes or snow, or atmospheric parameters, which all vary throughout the year, are not sufficiently represented within the method's covariance matrix. Due to this seasonal variation, the correction method used over Ecuador is inappropriate. The correction is also complicated by near-continuous volcanic activity in the Kamchatka region, and both volcanic (e.g., from the Kasatochi and Sarychev Peak eruptions) and anthropogenic (pollution from China) emissions carried into the region.

Instead, each month has been individually corrected with the following steps. (1) The data are again gridded to a 0.125° by 0.125° grid box and the orbits averaged for each month but this time removing pixels which are flagged as containing SO_2 by the linear retrieval, Figure 3g. (2) For each individual month, an average SO_2 free column amount is calculated for the northern Kamchatka region and this is used to correct for the bias in that month: shifting the SO_2 free distribution for the month to be centered at 0. An example from September 2010 is shown in the histogram in Figure 3e: the blue histogram shows before the correction value has been applied and the red shows the distribution following the correction. A before and after of the average SO_2 column amounts is shown in Figures 3f and 3h.

3.3.3. Arc-Scale Observations

As with Ecuador, the iterative retrieval output over Kamchatka was gridded to a 0.125° latitude by 0.125° longitude grid and averaged for each month (again incorporating both the morning and evening overpasses). These results are shown in Figure S2 in the supporting information. During the period examined emissions could be identified at each of the five volcanoes in the region; however, in some cases the signal was faint and so it is only with existing knowledge of volcanic activity in the region that these could be identified. In other cases, it was also difficult to discern which volcano the plumes originated from, without information from alternative sources, such as the GVP reports and other literature, due to the close proximity of volcanoes in the region.

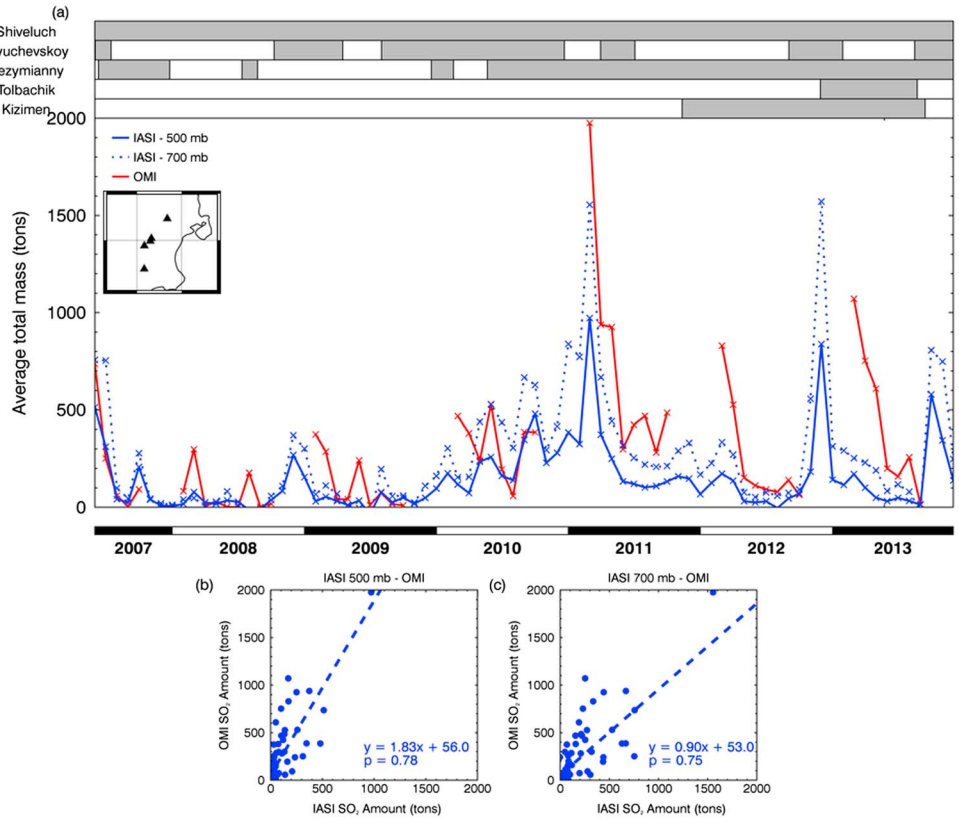

Figure 6. (a) Time series of average total SO_2 in the northern Kamchatka region calculated for the Infrared Atmospheric Sounding Interferometer (IASI; assuming plume heights of 500 and 700 mb) and the Ozone Monitoring Instrument (OMI). Eruptive periods as defined by the Global Volcanism Program are displayed at the top. (b) Scatterplot comparing the average total SO_2 mass obtained with the IASI and OMI retrievals, with the IASI retrieval assuming a plume height of 500 mb. (c) Same as (b) with the IASI retrieval assuming a plume altitude of 700 mb.

The results for 3 months, October 2007, June 2010, and July 2011, are presented in Figures 4g–4l alongside the results from the OMI retrieval. In each of these, volcanic plumes can be identified. However, as before, the plumes observed with OMI are significantly larger than those seen with IASI. This difference is reflected in Figure 6, which shows the average total mass calculated for the northern Kamchatka region for both instruments. Note that the mass has been calculated for the entire region, rather than for individual volcanoes due to the frequency with which plumes span multiple volcanic centers. The discrepancy between the results for the two instruments could be related to the different detection limits of the two instruments. The IASI iterative retrieval may also underestimate if the gas is beneath a thick ash or meteorological cloud or if the true height of the plume is less than the altitude assumed in the retrieval. For example, in this part of Kamchatka, the volcano heights vary between less than 3,000 m to closer to 5,000 m; see Table 2. Therefore, the altitude assumption of 500 mb (~5,600m) may be incorrect. To demonstrate the impact of this, the retrieval was also run using a fixed altitude of 700 mb (roughly 2.5 km), which led to increased SO_2 average total mass values as seen in Figure 6. It is also possible for the OMI DOAS retrieval to overestimate the SO_2 mass, if, for example, there was a highly reflective surface, such as snow, ice, or cloud, beneath the SO_2 plume.

Despite the discrepancy between the IASI and OMI results, reasonably high correlation coefficients of 0.78 and 0.75 were obtained for IASI-OMI combination with the 500 and 700-mb plume height assumption for the IASI retrieval, respectively, and while the average SO_2 mass magnitudes may not be the same; looking at Figure 6, it is apparent that both instruments are observing the same peaks in activity. Results are also available from the iterative retrieval during the winter months when there is no sunlight. During November and December 2012, for example, emissions can be seen from Tolbachik following a dual fissure eruption (GVP, 2012b). During these months, OMI and other UV sensors are unable to obtain data due to the lack of sunlight. It is therefore recommended that IASI should be used to compliment existing UV retrievals, particularly during winter months, to better understand ongoing activity.

4. Conclusions and Further Work

Previous applications of retrievals developed for IASI have been to larger eruptions, while few studies exist looking at smaller emissions of SO_2 into the troposphere, such as those from smaller explosive eruptions, noneruptive volcanic degassing, and emissions from anthropogenic sources. This study has demonstrated that there is some potential for using the infrared sensor IASI for both identifying emissions and for assessing long-term changes in SO_2 in different regions.

The linear retrieval applied here is a fast method for scanning large data sets for elevated levels of SO_2. The results shown in this paper were largely dominated by emissions from large eruptions such as Kasatochi, Sarychev Peak, and Nabro. However, emissions could also be identified from smaller sources, including both ongoing eruptive activity and smaller explosive eruptions. Signals were also identified from anthropogenic activity, such as from coal burning and copper smelting. These results demonstrate that there is potential for using this retrieval for detecting volcanic emissions, which could be done for rapid identification of SO_2 plumes in near real time or to highlight regions for further study. The results presented here are by no means a full catalog of emissions which are detectable with IASI, and future work is encouraged to fully appreciate the strengths and limitations of this method across the globe, to determine how successfully this can be applied to monitor volcanic emissions. The technique could also be further enhanced by forming local covariance matrices which better represent the background variability of a specific region or through the use of techniques such as plume rotation to enhance the result and improve source detection.

Following the identification of SO_2 emissions with the linear retrieval, a slower, but fully quantitative iterative retrieval can be applied to compute the SO_2 column amounts in a selected region. Here this has been applied over Ecuador and Kamchatka, both regions containing numerous active volcanoes. The quantification of emissions was initially complicated by prominent negative column amounts across both regions which had not been identified in previous applications of the iterative retrieval (applications to larger eruptions), probably linked to poor representation of background variability in these regions within the covariance matrix used. Two different methods for correcting this bias are presented. The first is a pixel-specific correction suitable in regions where the bias is spatially and temporally consistent, while the second is based on the monthly mean column amount for the region after pixels containing SO_2 have been removed, suitable when there is significant seasonal variability in the results. Following the removal of this bias, it is shown that the iterative retrieval results are able to capture relative changes in volcanic activity. Although the magnitude of the average total SO_2 masses differs between IASI and OMI (possibly related to the different detection limits, the plume altitude assumption, and the temperature contrast between the Earth's surface and the lower part of the atmosphere) the trends observed by these and ground-based DOAS measurements at Tungurahua agree well and matched episodes of activity noted in existing literature. This is also generally true for IASI and OMI in Kamchatka. Here the IASI instrument is capable of obtaining data in winter and so could be used to compliment OMI by filling this winter gap in their record. Further long-term studies of emissions at different volcanoes and at different time intervals would improve understanding of the advantages and disadvantages of this tool.

Retrievals developed for IASI are not commonly applied to volcanic emissions into the troposphere or to assess long-term changes in volcanic activity. The results presented here have demonstrated that the linear retrieval can identify multiple source types across the globe and that quantification of SO_2 amounts in individual regions with the iterative retrieval can show relative changes in volcanic activity. Numerous other signals, volcanic and anthropogenic, were identified in the linear retrieval results, and this could inspire similar long-term studies with the iterative retrieval. This study opens a number of promising avenues for further work, and such work would be valuable for both understanding volcanic activity and for appreciating the strengths and limitations of the IASI retrievals.

Acknowledgments
The IASI spectra used in this study are available from the Centre for Environmental Data Analysis (CEDA; EUMETSAT, 2009). The linear retrieval monthly average effective SO_2 column amounts on which this study was based are available as a data set (Taylor et al., 2018) at CEDA. J. P. was supported by a Met Office Academic Partnership. I. A. T. acknowledges the funding of NERC (NE/L002612/1). I. A. T., E. C., T. A. M., and R. G. G. are all supported by NERC Centre for Observation and Modelling of Earthquakes, Volcanoes, and Tectonics (COMET). E. C., R. G. G., and T. A. M. acknowledge funding from the NERC SHIVA project (NE/J023310/1). R. G. G. acknowledges funding from the NERC VANAHEIM project (NE/1015592/1). The authors would like to thank the reviewers for their constructive comments which have greatly improved the manuscript.

References

Aiuppa, A., Giudice, G., Liuzzo, M., Tamburello, G., Allard, P., Calabrese, S., et al. (2012). First volatile inventory for Gorely volcano, Kamchatka. *Geophysical Research Letters*, *39*, L06307. https://doi.org/10.1029/2012GL051177

Andres, R., & Kasgnoc, A. D. (1998). A time-averaged inventory of subaerial volcanic sulfur emissions. *Journal of Geophysical Research: Atmospheres*, *103*(D19), 25,251–25,261. https://doi.org/10.1029/98JD02091

Arellano, S., Galle, B., & Melnikov, D. (2012). Gas flux measurements of episodic bimodal eruptive activity at Karymsky volcano (Kamchatka, Russia). In *EGU General Assembly Conference Abstracts* (8325 pp.), Vienna, Austria.

Arellano, S. R., Hall, M., Samaniego, P., Le Pennec, J.-L., Ruiz, A., Molina, I., & Yepes, H. (2008). Degassing patterns of Tungurahua volcano (Ecuador) during the 1999–2006 eruptive period, inferred from remote spectroscopic measurements of SO_2 emissions. *Journal of Volcanology and Geothermal Research*, *176*(1), 151–162. https://doi.org/10.1016/j.jvolgeores.2008.07.007

Bauduin, S., Clarisse, L., Clerbaux, C., Hurtmans, D., & Coheur, P.-F. (2014). IASI observations of sulfur dioxide (SO_2) in the boundary layer of Norilsk. *Journal of Geophysical Research: Atmospheres*, *119*, 4253–4263. https://doi.org/10.1002/2013JD021405

Bauduin, S., Clarisse, L., Hadji-Lazaro, J., Theys, N., Clerbaux, C., & Ceheur, P.-F. (2016). Retrieval of near-surface sulfur dioxide (SO_2) concentrations at a global scale using IASI satellite observations. *Atmospheric Measurement Techniques*, *9*, 721–740. https://doi.org/10.5194/amt-9-721-2016

Blumstein, D., Chalon, G., Carlier, T., Buil, C., Hebert, P., Maciaszek, T., et al. (2004). IASI instrument: Technical overview and measured performances. *Proceedings of SPIE—The International Society of the Optical Engineering*, *5543*, 196–207. https://doi.org/10.1117/12.560907

Boichu, M., Menut, L., Khvorostyanov, D., Clarisse, L., Clerbaux, C., Turquety, S., & Coheur, P.-F. (2013). Inverting for volcanic SO_2 flux at high temporal resolution using spaceborne plume imagery and chemistry-transport modelling: The 2010 Eyjafjallajökull eruption case study. *Atmospheric Chemistry and Physics*, *13*(17), 8569–8584. https://doi.org/10.5194/acp-13-8569-2013

Campion, R., Salerno, G. G., Coheur, P.-F., Hurtmans, D., Clarisse, L., Kazahaya, K., et al. (2010). Measuring volcanic degassing of SO_2 in the lower troposphere with ASTER band ratios. *Journal of Volcanology and Geothermal Research*, *194*(1-3), 42–54. https://doi.org/10.1016/j.jvolgeores.2010.04.010

Carboni, E., Grainger, R., Walker, J., Dudhia, A., & Siddans, R. (2012). A new scheme for sulphur dioxide retrieval from IASI measurements: Application to the Eyjafjallajökull eruption of April and May 2010. *Atmospheric Chemistry and Physics*, *12*(23), 11,417–11,434. https://doi.org/10.5194/acp-12-11417-2012

Carboni, E., Grainger, R. G., Mather, T. A., Pyle, D. M., Thomas, G., Siddans, R., et al. (2016). The vertical distribution of Volcanic SO_2 plumes measured by IASI. *Atmospheric Chemistry and Physics*, *16*, 4343–4367. https://doi.org/10.5194/acp-16-4343-2016

Carn, S. A. (2016). On the detection and monitoring of effusive eruptions using satellite SO_2 measurements. *Geological Society, London, Special Publications*, *426*, 277–292. https://doi.org/10.1144/SP426.28

Carn, S. A., Clarisse, L., & Prata, A. J. (2016). Multi-decadal satellite measurements of global volcanic degassing. *Journal of Volcanology and Geothermal Research*, *311*, 99–134. https://doi.org/10.1016/j.jvolgeores.2016.01.002

Carn, S. A., & Prata, F. J. (2010). Satellite-based constraints on explosive SO_2 release from Soufrière Hills Volcano, Montserrat. *Geophysical Research Letters*, *37*, L00E22. https://doi.org/10.1029/2010GL044971

Carn, S. A., Fioletov, V. E., McLinden, C. A., Li, C., & Krotkov, N. A. (2017). A decade of global volcanic SO_2 emissions measured from space. *Nature*, *7*, 44095. https://doi.org/10.1038/srep44095

Carn, S. A., Krotkov, N. A., Yang, K., & Krueger, A. J. (2013). Measuring global volcanic degassing with the Ozone Monitoring Instrument (OMI). *Geological Society, London, Special Publications*, *380*(1), 229–257. https://doi.org/10.1144/SP380.12

Carn, S. A, Krueger, A. J., Arellano, S., Krotkov, N. A., & Yang, K. (2008). Daily monitoring of Ecuadorian volcanic degassing from space. *Journal of Volcanology and Geothermal Research*, *176*(1), 141–150. https://doi.org/10.1016/j.jvolgeores.2008.01.029

Carn, S. A., Krueger, A. J., Krotkov, N., Yang, K., & Levelt, P. (2007). Sulfur dioxide emissions from Peruvian copper smelters detected by the Ozone Monitoring Instrument. *Geophysical Research Letters*, *34*, L09801. https://doi.org/10.1029/2006GL029020

Carn, S. A., Strow, L. L., de Souza-Machado, S., Edmonds, Y., & Hannon, S. (2005). Quantifying tropospheric volcanic emissions with AIRS: The 2002 eruption of Mt. Etna (Italy). *Geophysical Research Letters*, *32*, L02301. https://doi.org/10.1029/2004GL021034

Carn, S. A., Yang, K., Prata, A. J., & Krotkov, N. A. (2015). Extending the long-term record of volcanic SO_2 emissions with the Ozone Mapping and Profiler Suite nadir mapper. *Geophysical Research Letters*, *42*, 925–932. https://doi.org/10.1002/2014GL062437

Casadevall, T., Rose, W., Gerlach, T., Greenland, L. P., Ewert, J., Wunderman, R., & Symonds, R. (1983). Gas emissions and the eruption of Mt. St. Helens through 1982. *Science*, *221*(44618), 1383–1385. https://doi.org/10.1126/science.221.4618.1383

Clarisse, L., Coheur, P.-F., Prata, A. J., Hurtmans, D., Razavi, A., Phulpin, T., et al. (2008). Tracking and quantifying volcanic SO_2 with IASI, the September 2007 eruption at Jebel at Tair. *Atmospheric Chemistry and Physics*, *8*(24), 7723–7734. https://doi.org/10.5194/acp-8-7723-2008

Clarisse, L., Coheur, P.-F., Theys, N., Hurtmans, D., & Clerbaux, C. (2014). The 2011 Nabro eruption, a SO_2 plume height analysis using IASI measurements. *Atmospheric Chemistry and Physics*, *14*(6), 3095–3111. https://doi.org/10.5194/acp-14-3095-2014

Clarisse, L., Hurtmans, D., Clerbaux, C., Hadji-Lazaro, J., Ngadi, Y., & Coheur, P.-F. (2012). Retrieval of sulphur dioxide from the Infrared Atmospheric Sounding Interferometer (IASI). *Atmospheric Measurement Techniques*, *5*(3), 581–594. https://doi.org/10.5194/amt-5-581-2012

Clark, T. L., Lopez, T. M., & Ushakov, S. (2007). Sulfur dioxide emissions from Bezymianny Volcano, Kamchatka: Results from the 2007 Field Season. *AGU Fall Meeting Abstracts*, *1*, 606.

Clerbaux, C., Boynard, A., Clarisse, L., George, M., Hadji-Lazaro, J., Herbin, H., et al. (2009). Monitoring of atmospheric composition using the thermal infrared IASI/MetOp sounder. *Atmospheric Chemistry and Physics*, *9*(16), 6041–6054. https://doi.org/10.5194/acp-9-6041-2009

Cooke, M. C., Francis, P. N., Millington, S., Saunders, R., & Witham, C. (2014). Detection of the Grímsvötn 2011 volcanic eruption plumes using infrared satellite measurements. *Atmospheric Science Letters*, *15*(4), 321–327. https://doi.org/10.1002/asl2.506

Corradini, S., Merucci, L., & Prata, A. J. (2009). Retrieval of SO_2 from thermal infrared satellite measurements: Correction procedures for the effects of volcanic ash. *Atmospheric Measurement Techniques*, *2*(1), 177–191. https://doi.org/10.5194/amt-2-177-2009

Corradini, S., Merucci, L., Prata, A. J., & Piscini, A. (2010). Volcanic ash and SO_2 in the 2008 Kasatochi eruption: Retrievals comparison from different IR satellite sensors. *Journal of Geophysical Research: Atmospheres*, *115*, D00L21. https://doi.org/10.1029/2009JD013634

Dean, K., & Dehn, J. (2015). *Monitoring volcanoes in the North Pacific: Observations from space*. Berlin: Springer.

Deeter, M. N., Edwards, D. P., Gille, J. C., & Drummond, J. (2007). Sensitivity of MOPITT observations to carbon monoxide in the lower troposphere. *Journal of Geophysical Research*, *112*, D24306. https://doi.org/10.1029/2007JD008929

Delgado Granados, H., & Cardenas Gonzalez, L (2013). ~ 20 years of SO_2 measurements at Popocatépetl volcano (Mexico) using COSPEC: Volcanological interpretation of the data and use for validation of instrumental developments. *AGU Fall Meeting Abstracts*, *1*, 2874.

Edmonds, M. (2008). New geochemical insights into volcanic degassing. *Philosophical Transactions of the Royal Society A: Mathematical, Physical and Engineering Sciences*, *366*(1885), 4559–4579. https://doi.org/10.1098/rsta.2008.0185

Edmonds, M., Herd, R. A., Galle, B., & Oppenheimer, C. M. (2003). Automated, high time-resolution measurements of SO_2 flux at Soufrière Hills Volcano, Montserrat. *Bulletin of Volcanology*, *65*(8), 578–586. https://doi.org/10.1007/s00445-003-0286-x

Eisinger, M., & Burrows, J. P. (1998). Tropospheric sulfur dioxide observed by the ERS-2 GOME instrument. *Geophysical Research Letters*, *25*(22), 4177–4180. https://doi.org/10.1029/1998GL900128

Elias, T., Sutton, A. J., Oppenheimer, C., Horton, K. A., Garbeil, H., Tsanev, V., et al. (2006). Comparison of COSPEC and two miniature ultraviolet spectrometer systems for SO_2 measurements using scattered sunlight. *Bulletin of Volcanology*, *68*(4), 313–322. https://doi.org/10.1007/s00445-005-0026-5

European Organisation for the Exploitation of Meteorological Satellites (2009). IASI: Atmospheric sounding Level 1C data products. NERC Earth Observation Data Centre, 27th March 2018. http://catalogue.ceda.ac.uk/ uuid/ea46600afc4559827f31dbfbb8894c2e

European Organisation for the Exploitation of Meteorological Satellites (2017). IASI, Website accessed in February 2017. http://www.eumetsat.int/website/home/Satellites/CurrentSatellites/Metop/MetopDesign/ IASI/index.html

Fioletov, V., McLinden, C., Krotkov, N., & Li, C. (2015). Lifetimes and emissions of SO_2 from point sources estimated from OMI. *Geophysical Research Letters*, *42*, 1969–1976. https://doi.org/10.1002/2015GL063148

Fioletov, V., McLinden, C. A., Krotkov, N., Li, C., Joiner, J., Theys, N., et al. (2016). A global catalogue of large SO_2 sources and emissions derived from the Ozone Monitoring Instrument. *Atmospheric Chemistry and Physics*, *16*, 11,497–11,519. https://doi.org/10.5194/acp-16-11497-2016

Fioletov, V. E., McLinden, C. A., Krotkov, N., Yang, K., Loyola, D. G., Valks, P., et al. (2013). Application of OMI, SCIAMACHY, and GOME-2 satellite SO_2 retrievals for detection of large emission sources. *Journal of Geophysical Research: Atmospheres*, *118*, 11,399–11,418. https://doi.org/10.1002/jgrd.50826

Fischer, T. P., Morrissey, M. M., Calvache, V. M. L., Gomez, M. D., Torres, C. R., Stix, J., & Williams, S. N. (1994). Correlations between SO_2 flux and long-period seismicity at Galeras volcano. *Nature*, *368*(6467), 135–137. https://doi.org/10.1038/368135a0

Galle, B., Johansson, M., Rivera, C., Zhang, Y., Kihlman, M., Kern, C., et al. (2010). Network for Observation of Volcanic and Atmospheric Change (NOVAC)—A global network for volcanic gas monitoring: Network layout and instrument description. *Journal of Geophysical Research: Atmospheres*, *115*, D05304. https://doi.org/10.1029/2009JD011823

Galle, B., Oppenheimer, C., Geyer, A., McGonigle, A. J. S., Edmonds, M., & Horrocks, L. (2003). A miniaturised ultraviolet spectrometer for remote sensing of SO_2 fluxes: A new tool for volcano surveillance. *Journal of Volcanology and Geothermal Research*, *119*(1), 241–254. https://doi.org/10.1016/S0377-0273(02)00356-6

Grutter, M., Basaldud, R., Rivera, C., Harig, R., Junkerman, W., Caetano, E., & Delgado Granados, H. (2008). SO_2 emissions from Popocatépetl volcano: Emission rates and plume imaging using optical remote sensing techniques. *Atmospheric Chemistry and Physics*, *8*, 6655–6663.

Global Volcanism Program (1999). Report on Guagua Pichincha (Ecuador). In R. Wunderman (Ed.), *Bulletin of the Global Volcanism Network* (Vol. 24, no. 2). Smithsonian Institution.

Global Volcanism Program (2009). Report on Reventador (Ecuador). In R. Wunderman (Ed.), *Bulletin of the Global Volcanism Network* (Vol. 34, no. 3). Smithsonian Institution.

Global Volcanism Program (2009). Report on Galeras (Colombia). In R. Wunderman (Ed.), *Bulletin of the global volcanism network* (Vol. 34, no. 7). Smithsonian Institution.

Global Volcanism Program (2010a). Report on Klyuchevskoy (Russia). In R. Wunderman (Ed.), *Bulletin of the global volcanism network* (Vol. 35, no. 6). Smithsonian Institution.

Global Volcanism Program (2010b). Report on Sheveluch (Russia), *Bulletin of the global volcanism network* (Vol. 35, no. 3). Smithsonian Institution.

Global Volcanism Program (2010c). Report on Sheveluch (Russia). In S. K. Sennert (Ed.), *Weekly volcanic activity report, 3 November–9 November 2010*: Smithsonian Institution and US Geological Survey.

Global Volcanism Program (2012a). Report on Nevado del Huila (Colombia). In R. Wunderman (Ed.), *Bulletin of the global volcanism network* (Vol. 37, no. 10). Smithsonian Institution.

Global Volcanism Program (2012b). Report on Tolbachik (Russia). In R. Wunderman (Ed.), *Bulletin of the global volcanism network* (Vol. 37, no. 12). Smithsonian Institution.

Global Volcanism Program (2013a). Report on Klyuchevskoy (Russia), *Bulletin of the global volcanism network* (Vol. 38, no. 7). Smithsonian Institution.

Global Volcanism Program (2013b). Report on Galeras (Colombia). In Wunderman, R. (Ed.), *Bulletin of the global volcanism network* (Vol. 38, no. 3). Smithsonian Institution.

Global Volcanism Program (2013c). Report on Tungurahua (Ecuador). In Sennert, S. K. (Ed.), *Weekly volcanic activity report, 16 October–22 October 2013, Smithsonian Institution and US Geological Survey*.

Global Volcanism Program (2013d). Report on Tungurahua (Ecuador). In S. K. Sennert (Ed.), *Weekly volcanic activity report, 30 October–5 November 2013*: Smithsonian Institution and US Geological Survey.

Global Volcanism Program (2013e). Report on Tungurahua (Ecuador). In S. K. Sennert (Ed.), *Weekly volcanic activity report, 6 November–12 November 2013*: Smithsonian Institution and US Geological Survey.

Halmer, M., Schmincke, H.-U., & Graf, H.-F. (2002). The annual volcanic gas input into the atmosphere, in particular into the stratosphere: A global data set for the past 100 years. *Journal of Volcanology and Geothermal Research*, *115*(3), 511–528.

Haywood, J. M., Jones, A., Clarisse, L., Bourassa, A., Barnes, J., Telford, P., et al. (2010). Observations of the eruption of the Sarychev volcano and simulations using the HadGEM2 climate model. *Journal of Geophysical Research*, *115*, D21212. https://doi.org/10.1029/2010JD014447

Heard, I. P. C., Manning, A. J., Haywood, J. M., Witham, C., Redington, A., Jones, A., et al. (2012). A comparison of atmospheric dispersion model predictions with observations of SO_2 and sulphate aerosol from volcanic eruptions. *Journal of Geophysical Research*, *117*, D00U22. https://doi.org/10.1029/2011JD016791

Hidalgo, S., Battaglia, J., Arellano, S., Steele, A., Bernard, B., Bourquin, J., et al. (2015). SO_2 degassing at Tungurahua volcano (Ecuador) between 2007 and 2013: Transition from continuous to episodic activity. *Journal of Volcanology and Geothermal Research*, *298*(0), 1–14. https://doi.org/10.1016/j.jvolgeores.2015.03.022

Horton, K. A., Williams-Jones, G., Garbeil, H., Elias, T., Sutton, A. J., Mouginis-Mark, P., et al. (2006). Real-time measurement of volcanic SO_2 emissions: Validation of a new UV correlation spectrometer (FLYSPEC). *Bulletin of Volcanology*, *68*(4), 323–327. https://doi.org/10.1007/s00445-005-0014-9

Karagulian, F., Clarisse, L., Clerbaux, C., Prata, A. J., Hurtmans, D., & Coheur, P.-F. (2010). Detection of volcanic SO_2, ash, and H_2SO_4 using the Infrared Atmospheric Sounding Interferometer (IASI). *Journal of Geophysical Research*, *115*, D00L02. https://doi.org/10.1029/2009JD012786

Klimont, Z., Smith, S. J., & Cofala, J. (2013). The last decade of global anthropogenic sulfur dioxide: 2000–2011 emissions. *Environmental Research Letters*, *8*, 014003. https://doi.org/10.1088/1748-9326/8/1/014003

Koukouli, M. E., Balis, D. S., der van A, R. J., Theys, N., Hedelt, P., Richter, A., et al. (2016). Anthropogenic SO_2 load over China as observed from different satellite sensors. *Atmospheric Environment*, *145*, 45–59. https://doi.org/10.1016/j.atmosenv.2016.09.007

Koukouli, M. E., Clarisse, L., Carboni, E., Van Gent, J., Spinetti, C., Balis, D., et al. (2015). Intercomparison of Metop-A SO_2 measurements during the 2010–2011 Icelandic eruptions. *Annals of Geophysics*, *57*, 1–6. https://doi.org/10.4401/ag-6613.

Krotkov, N. A., McLinden, C. A., Li, C., Lamsal, L. N., Celarier, E. A., Marchenko, S. V., et al. (2016). Aura OMI observations of regional SO_2 and NO_2 pollution changes from 2005 to 2015. *Atmospheric Chemistry and Physics*, *16*, 4605–4629. https://doi.org/10.5194/acp-16-4605-2016

Krueger, A. J. (1983). Sighting of El Chichón sulfur dioxide clouds with the Nimbus 7 total ozone mapping spectrometer. *Science*, *220*(4604), 1377–1379. https://doi.org/10.1126/science.220.4604.1377

Krueger, A., Krotkov, N., & Carn, S. (2008). El Chichón: The genesis of volcanic sulfur dioxide monitoring from space. *Journal of Volcanology and Geothermal Research*, *175*(4), 408–414. https://doi.org/10.1016/j.jvolgeores.2008.02.026

Lopez, T., Fee, D., Prata, F., & Dehn, J. (2013). Characterization and interpretation of volcanic activity at Karymsky Volcano, Kamchatka, Russia, using observations of infrasound, volcanic emissions, and thermal imagery. *Geochemistry, Geophysics, Geosystems*, *14*, 5106–5127. https://doi.org/10.1002/2013GC004817

Malinconico, L. (1979). Fluctuations in SO_2 emission during recent eruptions of Etna. *Nature*, *278*, 43–45. https://doi.org/10.1038/278043a0

McCormick, B. T., Edmonds, M., Mather, T. A., Campion, R., Hayer, C. S., Thomas, H. E., & Carn, S. A. (2013). Volcano monitoring applications of the Ozone Monitoring Instrument. *Geological Society, London, Special Publications*, *380*(1), 259–291. http://doi.org/10.1144/SP380.11

McCormick, B. T., Herzog, M., Yang, J., Edmonds, M., Mather, T. A., Carn, S. A., et al. (2014). A comparison of satellite-and ground-based measurements of SO_2 emissions from Tungurahua volcano, Ecuador. *Journal of Geophysical Research: Atmospheres*, *119*, 4264–4285. https://doi.org/10.1002/2013JD019771

McGonigle, A. J. S., Oppenheimer, C., Galle, B., Mather, T. A., & Pyle, D. M. (2002). Walking traverse and scanning DOAS measurements of volcanic gas emission rates. *Geophysical Research Letters*, *29*(20), 1985. https://doi.org/10.1029/2002GL015827

McGonigle, A. J. S., Oppenheimer, C., Tsanev, V. I., Saunders, S., Mulina, K., Tohui, S., et al. (2004). Sulphur dioxide fluxes from Papua New Guinea's volcanoes. *Geophysical Research Letters*, *31*, L08606. https://doi.org/10.1029/2004GL019568

Melnikov, D., Ushakov, S., & Galle, B. (2014). Estimation of the sulfur dioxide emission by Kamchatka volcanoes using differential optical absorption spectroscopy. In *Workshop on Japan-Kamchatka-Alaska Subduction Processes*, pp. 8.

Menard, G., Moune, S, Vlastélic, I., Aguilera, F., Valade, S., Bontemps, M., & Gonzàlez, R. (2014). Gas and aerosol emissions from Lascar volcano (Northern Chile): Insights into the origin of gases and their links with the volcanic activity. *Journal of Volcanology and Geothermal Research*, *287*, 51–67. https://doi.org/10.1016/j.jvolgeores.2014.09.004

Moffat, A. J., & Millán, M. M. (1971). The application of optical correlation techniques to the remote sensing of SO_2 plumes using skylight. *Atmospheric Environment*, *5*(8), 677–690. https://doi.org/10.1016/0004-6981(71)90125-9

Moxnes, E. D., Kristiansen, N. I., Stohl, A., Clarisse, L., Durant, A., Weber, K., & Vogel, A. (2014). Separation of ash and sulfur dioxide during the 2011 Grímvötn eruption. *Journal of Geophysical Research: Atmospheres*, *119*, 7477–7501. https://doi.org/10.1002/2013JD021129

Neal, C. A., Herrick, J., Girina, O. A., Chibisova, M., Rybin, A., McGimsey, R. G., & Dixon, J. (2014). 2010 Volcanic activity in Alaska, Kamchatka, and the Kurile Islands: Summary of events and response of the Alaska Volcano Observatory (*Scientific Investigations Report 2014-5034*). U.S. Department of the Interior U.S. Geological Survey.

Novak, M. A. M., Watson, I. M., Delgado-Granados, H., Rose, W. I., Cárdenas-González, L., & Realmuto, V. J. (2008). Volcanic emissions from Popocatépetl volcano, Mexico, quantified using Moderate Resolution Imaging Spectroradiometer (MODIS) infrared data: A case study of the December 2000–January 2001 emissions. *Journal of Volcanology and Geothermal Research*, *170*(1-2), 76–85. https://doi.org/10.1016/j.jvolgeores.2007.09.010

Oppenheimer, C. (2010). Ultraviolet sensing of volcanic sulfur emissions. *Elements*, *6*(2), 87–92. https://doi.org/10.2113/gselements.6.2.87

Oppenheimer, C., Fischer, T. P., & Scaillet, B. (2014). Volcanic degassing: Process and impact, *Treatise on Geochemistry* (pp. 111–179). Amsterdam, Netherlands: Elsevier.

Oppenheimer, C., Scaillet, B., & Martin, R. S. (2011). Sulfur degassing from volcanoes: Source conditions, surveillance, plume chemistry and earth system impacts. *Reviews in Mineralogy and Geochemistry*, *73*(1), 363–421. https://doi.org/10.2138/rmg.2011.73.13

Prata, A. J., & Bernardo, C. (2007). Retrieval of volcanic SO_2 column abundance from Atmospheric Infrared Sounder data. *Journal of Geophysical Research*, *112*, D20204. https://doi.org/10.1029/2006JD007955

Prata, A. J., Carn, S. A., Stohl, A., & Kerkmann, J. (2007). Long range transport and fate of a stratospheric volcanic cloud from Soufrière hills volcano, Montserrat. *Atmospheric Chemistry and Physics*, *7*(19), 5093–5103. https://doi.org/10.5194/acp-7-5093-2007

Prata, A. J., & Kerkmann, J. (2007). Simultaneous retrieval of volcanic ash and SO_2 using MSG-SEVIRI measurements. *Geophysical Research Letters*, *34*, L05813. https://doi.org/10.1029/2006GL028691

Prata, A. J., Rose, W. I., Self, S., & O'Brien, D. M. (2003). Global, long-term sulphur dioxide measurements from TOVS data: A new tool for studying explosive volcanism and climate, *Volcanism and the Earth's Atmosphere* (pp. 75–92). Washington, DC: American Geophysical Union. https://doi.org/10.1029/139gm05

Pugnaghi, S., Gangale, G., Corradini, S., & Buongiorno, M. F. (2006). Mt. Etna sulfur dioxide flux monitoring using ASTER-TIR data and atmospheric observations. *Journal of Volcanology and Geothermal Research*, *152*(1-2), 74–90. https://doi.org/10.1016/j.jvolgeores.2005.10.004

Realmuto, V., Sutton, A. J., & Elias, T. (1997). Multispectral imaging of sulfur dioxide plumes from the East Rift Zone of Kilauea Volcano, Hawaii. *Journal of Geophysical Research*, *102*(B7), 15,057–15,072. https://doi.org/10.1029/96JB03916

Realmuto, V. J. (2000). The potential use of Earth Observing System data to monitor the passive emission of sulfur dioxide from volcanoes. *Geophysical Monograph Series*, *116*, 101–115. https://doi.org/10.1029/GM116p0101

Realmuto, V. J., Abrams, M., Buongiornio, M., & Pieri, D. (1994). The use of multispectral thermal infrared image data to estimate the sulfur dioxide flux from volcanoes: A case study from Mount Etna, Sicily, 29 July 1986. *Journal of Geophysical Research*, *99*(B1), 481–488. https://doi.org/10.1029/93JB02062

Rivera, M., Jean-Claude, T., Mariño, J., Berolatti, R., & Fuentes, J. (2010). Characteristics and management of the 2006–2008 volcanic crisis at the Ubinas volcano (Peru). *Journal of Volcanology and Geothermal Research*, *198*(1-2), 19–34. https://doi.org/10.1016/j.jvolgeores.2010.07.020

Rix, M., Valks, P., Hao, N., van Geffen, J., Clerbaux, C., Clarisse, L., et al. (2009). Satellite monitoring of volcanic sulfur dioxide emissions for early warning of volcanic hazards. *IEEE Journal of Selected Topics in Applied Earth Observations and Remote Sensing*, *2*(3), 196–206. https://doi.org/10.1109/JSTARS.2009.2031120

Scaillet, B., Clemente, B., Evans, B. W., & Pichavant, M. (1998). Redox control of sulfur degassing in silicic magmas. *Journal of Geophysical Research*, *103*(B10), 23,937–23,949. https://doi.org/10.1029/98JB02301

Stoiber, R., Malinconico, L., & Williams, S. (1983). *Use of the correlation spectrometer at volcanoes* (pp. 425–444). Amsterdam, Netherlands: Elsevier.

Surono, P. J., Pallister, J., Boichu, M., Buongiorno, M. F., Budisantoso, A., Costa, F., et al. (2012). The 2010 explosive eruption of Java's Merapi volcano—A 100-year event. *Journal of Volcanology and Geothermal Research*, *241*, 121–135. https://doi.org/10.1016/j.jvolgeores.2012.06.018

Symonds, R. B., Rose, W. I., Bluth, G. J., & Gerlach, T. M. (1994). Volcanic-gas studies; methods, results, and applications. *Reviews in Mineralogy and Geochemistry*, *30*(1), 1–66.

Taran, Y. A. (2009). Geochemistry of volcanic and hydrothermal fluids and volatile budget of the Kamchatka-Kuril subduction zone. *Geochimica et Cosmochimica Acta*, *73*(4), 1067–1094.

Taylor, I. A., Carboni, E., & Grainger, R. G. (2018). IASI global monthly averages of effective sulphur dioxide (SO_2) column amounts, 2007–2014, version 1.0. *Centre for Environmental Data Analysis*. https://doi.org/10.5285/8eb35b1ab1b2476986d174a2f0231307

Theys, N., Campion, R., Clarisse, L., Brenot, H., Van Gent, J., Dils, B., et al. (2013). Volcanic SO_2 fluxes derived from satellite data: A survey using OMI, GOME-2, IASI and MODIS. *Atmospheric Chemistry and Physics*, *13*(12), 5945–5968. https://doi.org/10.5194/acp-13-5945-2013

Theys, N., De Smedt, I., Gent, J., Danckaert, T., Wang, T., Hendrick, F., et al. (2015). Sulfur dioxide vertical column DOAS retrievals from the Ozone Monitoring Instrument: Global observations and comparison to ground-based and satellite data. *Journal of Geophysical Research: Atmospheres*, *120*, 2470–2491. https://doi.org/10.1002/2014JD022657

Thomas, H., & Watson, I. M (2010). Observations of volcanic emissions from space: Current and future perspectives. *Natural Hazards*, *54*(2), 323–354. https://doi.org/10.1007/s11069-009-9471-3

Urai, M. (2004). Sulfur dioxide flux estimation from volcanoes using advanced spaceborne thermal emission and reflection radiometer—A case study of Miyakejima volcano, Japan. *Journal of Volcanology and Geothermal Research*, *134*(1-2), 1–13. https://doi.org/10.1016/j.jvolgeores.2003.11.008

Walker, J., Carboni, E., Dudhia, A., & Grainger, R. (2012). Improved detection of sulphur dioxide in volcanic plumes using satellite-based hyperspectral infrared measurements: Application to the Eyjafjallajökull 2010 eruption. *Journal of Geophysical Research: Atmospheres*, *117*, D00U16. https://doi.org/10.1029/2011JD016810

Walker, J., Dudhia, A., & Carboni, E. (2011). An effective method for the detection of trace species demonstrated using the MetOp Infrared Atmospheric Sounding Interferometer. *Atmospheric Measurement Techniques*, *4*, 1567–1580. https://doi.org/10.5194/amt-4-1567-2011

Watson, I. M., Realmuto, V. J., Rose, W. I., Prata, A. J., Bluth, G. J. S., Gu, Y., et al. (2004). Thermal infrared remote sensing of volcanic emissions using the Moderate Resolution Imaging Spectroradiometer. *Journal of Volcanology and Geothermal Research*, *135*(1), 75–89. https://doi.org/10.1016/j.jvolgeores.2003.12.017